Author version

Published as:

Wang, B., Orndorff, N. C., Joshy, A. J., & Hwang, J. T. (2024). Graph-accelerated large-scale multidisciplinary design optimization under uncertainty of a laser-beam-powered aircraft. In AIAA SCITECH 2024 Forum (Paper No. AIAA 2024-0169). https://doi.org/10.2514/6.2024-0169

BibTeX for this reference:

https://lsdolab.github.io/lsdo-publications/publication/wang2024grapha/

```
@inproceedings{wang2024grapha,
  author = {Bingran Wang and Nicholas C. Orndorff and Anugrah J. Joshy and John T.
    Hwang},
  title = {Graph-accelerated large-scale multidisciplinary design optimization under
    uncertainty of a laser-beam-powered aircraft},
  booktitle = {AIAA SCITECH 2024 Forum},
  year = {2024},
  doi = {10.2514/6.2024-0169},
  url = {https://doi.org/10.2514/6.2024-0169}
}
```

AIAA SciTech Forum
8-12 January 2024, Orlando, FL
AIAA SCITECH 2024 Forum

10.2514/6.2024-0169

Graph-accelerated large-scale multidisciplinary design optimization under uncertainty of a laser-beam-powered aircraft

Bingran Wang*, Nicholas C. Orndorff†, Anugrah Jo Joshy ‡, and John T. Hwang§
University of California, San Diego, La Jolla, CA, 92093

Recently, the graph-accelerated non-intrusive polynomial chaos (NIPC) methods have been introduced to effectively address a variety of uncertainty quantification (UQ) challenges in multi-disciplinary and multi-point models. The essence of these graph-accelerated NIPC methods lies in leveraging tensor-grid input points for sampling the random space and using a computational graph transformation method, AMTC, to efficiently perform the tensor-grid evaluations by taking advantage of the inherent sparsity within the computational graph of the computational model. Despite their advancements, the effectiveness of these methods in tackling optimization under uncertainty (OUU) problems remains unexplored. This paper presents a detailed case study for a laser-beam-powered aircraft design problem. The focus is on applying the graph-accelerated NIPC methods to solve a large-scale multidisciplinary design optimization problem under uncertainty. This study not only compares the results of multidisciplinary optimization (MDO) and OUU but also highlights the effectiveness of the graph-accelerated NIPC method in tackling OUU challenges. The numerical results show that the OUU-optimized design is more robust under the variations of the flight conditions. Additionally, the AMTC method accelerates the optimization time by a factor of five, making the computational cost of the OUU problem only twice that of the MDO problem.

I. Introduction

Multidisciplinary design optimization (MDO) has gained popularity in both industry and academia due to its success in using numerical optimization techniques to find improved designs. Notably, MDO has been successful in designing aircraft [1, 2], automobiles [3, 4], wind turbines [1, 5], launch vehicles [6] and satellites [7, 8].

Widely used MDO software like OpenMDAO [9] and CSDL [10] rely on using gradient-based optimizer to find a local minimum for the optimization problems. These software tools currently require users to define the system as a computational model, with inputs and parameters defined as deterministic variables. However, in practice, computational models are always subject to uncertainties. Take the aircraft design problem as an example, the designed aircraft may need to operate at different flight conditions, and the computational solvers suffer from model errors associated with the computational methods we choose. Incorporating these uncertainties into optimization problems leads to optimization under uncertainty (OUU) problems, where objective and constraint functions are expressed as statistical moments or other risk measures of the stochastic output. A well-formulated OUU problem can result in a more realistic design that is robust and reliable under the variations of the identified uncertainties [11].

In the case of large-scale MDO problems, it may be necessary to perform numerous evaluations of the computational model, a process that can consume several hours or even days of computational resources. In contrast, the computational framework for OUU typically incorporates a nested UQ solver within the optimization process, leading to a significant escalation in computational costs when compared to deterministic MDO problems. Hence, the selection of an appropriate UQ method is paramount when addressing large-scale OUU problems.

In prior research, a range of UQ methodologies have been employed, including polynomial chaos [12, 13], kriging [14, 15], and Monte Carlo [16]. These UQ methods have been integrated with optimization algorithms to tackle OUU problems. Notably, recent advancements have sought to enhance the efficiency of these approaches through the incorporation of multi-fidelity [17, 18] and dimension reduction [19] techniques. Recently, Wang and Hwang introduced the graph-accelerated non-intrusive polynomial chaos method, which uses the integration-based non-intrusive polynomial chaos method with the tensor-grid quadrature rule to solve the UQ problem. Additionally, it uses a new

*Ph.D Candidate, Department of Mechanical and Aerospace Engineering, AIAA Student Member.
†Ph.D Student, Department of Mechanical and Aerospace Engineering, AIAA Student Member.
‡Ph.D Candidate, Department of Mechanical and Aerospace Engineering, AIAA Student Member.
§Assistant Professor, Department of Mechanical and Aerospace Engineering, AIAA Member.

computational graph transformation method, Accelerated Model evaluations on Tensor grids using Computational graph transformations (AMTC) method [20, 21], to accelerate the model evaluations on tensor-grid inputs. This combination has demonstrated exceptional efficiency, particularly when solving low-dimensional UQ problems. It capitalizes on the inherent sparsity present within the computational graphs of certain multidisciplinary and multi-point models.

In this paper, we employ the graph-accelerated NIPC method to address a specific large-scale multidisciplinary design optimization under uncertainty problem, stemming from a laser-beam-powered aircraft design scenario. The advancements in power-beaming technology have opened up possibilities for the development of unmanned aircraft primarily powered by laser beams. This breakthrough offers the potential to reduce the reliance on onboard energy storage, prompting the exploration of new aircraft designs that can fully leverage this unique property. Expanding upon previous research in MDO for similar aircraft, as discussed in [22], we develop a practical OUU problem tailored to a specific mission scenario. This problem formulation accounts for three pivotal random variables linked to flight conditions. The numerical results offer a comparative analysis of the designs optimized through MDO and OUU for specific metrics. The findings highlight that the OUU-optimized design exhibits greater robustness and reliability when subjected to the defined uncertain inputs. Furthermore, we demonstrate a substantial acceleration in optimization time, achieving a fivefold improvement by implementing the computational graph transformation method, AMTC. This efficiency enhancement results in a computational cost for solving the OUU problem that is merely double that of solving the MDO problem.

This paper is organized as follows. Section II describes the computational models and optimization formulations for the laser-beam-powered aircraft design problem. Section III presents the details of the graph-accelerated NIPC method and the implementation details on how it is used to solve the OUU problem. Section IV shows numerical results on this problem. Section V summarizes the work and offers concluding thoughts.

II. Problem setup

In this paper, we aim to optimize the conceptual design of a twin-fuselage, high-altitude unmanned airplane. This aircraft is uniquely engineered to accommodate a central pod that receives power from an incoming laser beam and converts it to electrical power via an internal photoelectric array. The airplane concept is shown in Fig. 1. We consider a simple mission scenario where the aircraft is in cruise condition while being powered only by a laser beam emitted from a ground station. The laser engagement scenario is shown in Fig. 2. The detailed descriptions for all of the sub-models for each discipline can be found in [22].

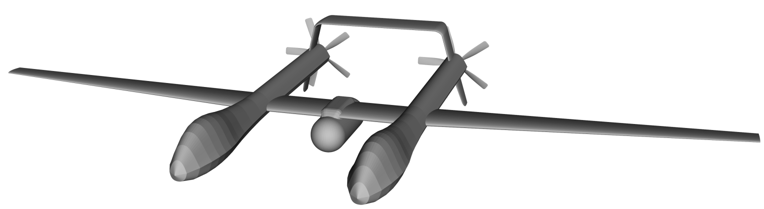

Fig. 1 The high-altitude, laser-powered airplane concept

A. Computational model and optimization formulations

Our computational model involves multiple disciplines, including aerodynamics, structural analysis, thermal dissipation, power beaming, and stability assessment. The aerodynamic solver employs the vortex-lattice method to calculate the aerodynamic forces generated by the wing and tail. In the structural analysis component, we assume a wing-box structure and determine the Von-Mises stress at specific evaluation points on the beam cross-section, focusing on areas where bending and shear stress are expected to be the greatest. For the power-beaming model, we leverage data generated from the High Energy Laser End-to-End Operational Simulation (HELEEOS) [23] software to compute beam propagation loss. The meshes used for the structure and aerodynamics solvers are both shown in Fig. 3 Additionally, Fig. 4 provides a visual representation of the wing box structure.

We begin by establishing an MDO problem, as outlined in [22]. The objective here is to find the optimal aircraft design, with a focus on minimizing the total weight of the aircraft while ensuring compliance with specified constraints. A detailed formulation of the MDO problem is presented in Tab. 1, and the associated XDSM diagram is depicted in Fig. 5. It's important to note that, in addition to the optimization constraints outlined in Tab. 1, several requirements

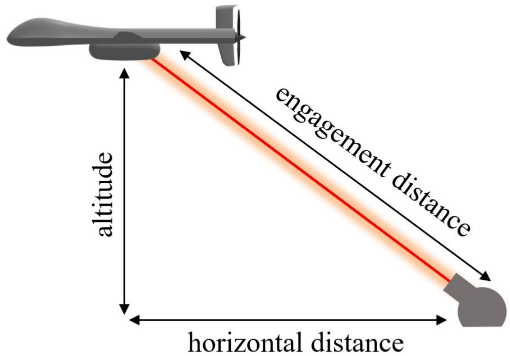

Fig. 2 The laser beam engagement scenario

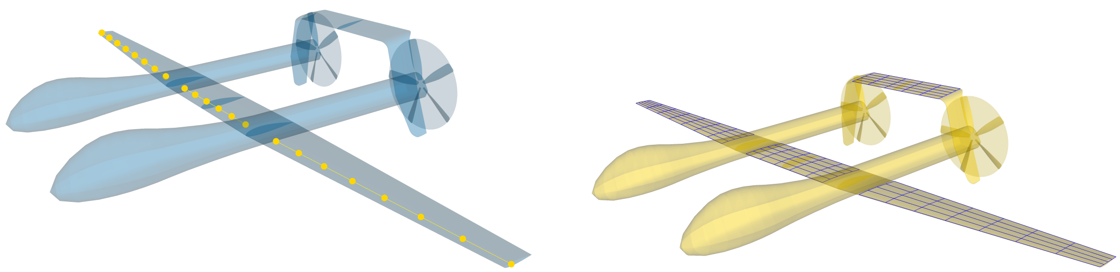

(a) 1D beam meshes for the structure solver **(b) 2D aerodynamics meshes for the aerodynamics solver**

Fig. 3 Meshes for structure and aerodynamics solvers

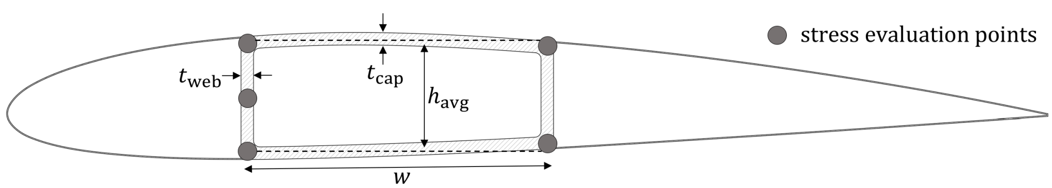

Fig. 4 The wing box structure with stree evaluation points

are inherently embedded within the computational model. These encompass considerations such as endurance, heat dissipation, and static margin, all of which contribute to shaping the final aircraft design.

Upon examination of the MDO formulation presented in Tab. 1, we identified three pivotal uncertain inputs: flight altitude, horizontal distance, and payload weight. These stochastic variables exhibit variability as the aircraft operates across diverse mission scenarios. To account for the variability of these three uncertain inputs within our optimization framework, we proceeded to formulate the OUU problem, as outlined in Tab. 2. This formulation adheres to the principles of robust design optimization, wherein the objective function and inequality constraints are expressed as linear combinations of the statistical moments of the stochastic outputs.

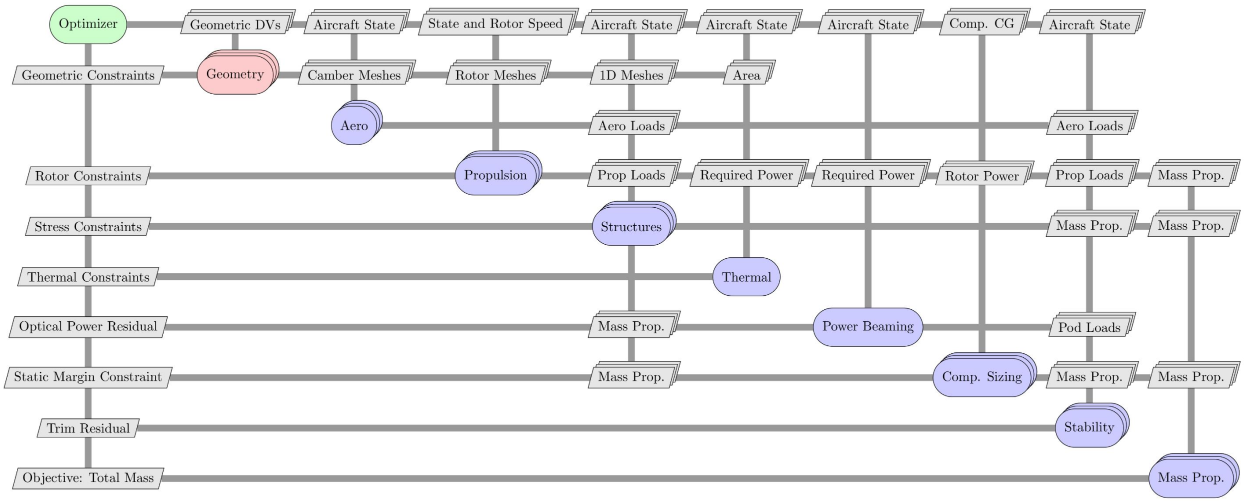

Fig. 5 XDSM diagram of the computational mdoel

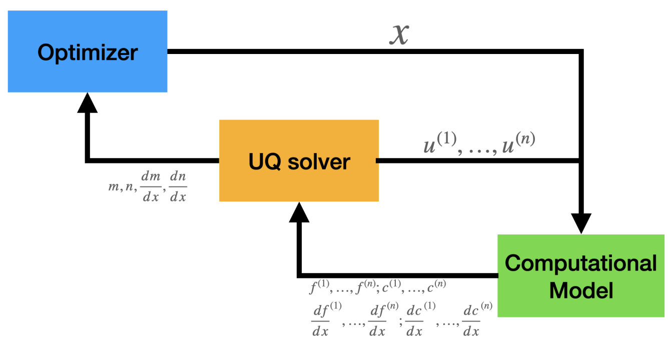

Fig. 6 Computational framework for gradient-based OUU problems

III. Graph-accelerated optimization under uncertainty

The OUU problem formulated in Tab. 2 can be written as

$$\begin{aligned} \min_{x} \quad & \mathcal{M}(x) := \mathbb{E}[f(x,U)] + 3\mathbb{S}[f(x,U)] \\ \text{subject to} \quad & \mathcal{N}(x) := \mathbb{E}[c(x,U)] + 3\mathbb{S}[c(x,U)] < 0 \\ & x_{lb} \leq x \leq x_{up}, \end{aligned} \tag{1}$$

where x represents the design variables with lower and upper bounds represented as x_{lb} and x_{up}, respectively. U represents the uncertain inputs. $\mathcal{M}$ and $\mathcal{N}$ represent the robust objective and robust constraint functions, respectively. These functions incorporate the statistical moments of stochastic outputs of the original objective and constraints functions, $f(x,U)$ and $c(x,U)$, respectively. We solve this optimization problem by connecting a UQ solver with a gradient-based optimizer in a nested for-loop approach, which is demonstrated in Fig. 6. In this approach, at each optimization iteration, we use a UQ solver to solve $\mathcal{M}$ and $\mathcal{N}$ and their gradients with respect to the design variables, $\frac{d\mathcal{M}}{dx}$ and $\frac{d\mathcal{N}}{dx}$. This information is passed into the optimizer to update the design variables.

A. Graph-accelerated non-intrusive polynomial chaos for uncertainty quantification

In this OUU problem, we need to solve a UQ problem at each optimization iteration. Therefore, the efficiency of the selected UQ method plays a crucial role in achieving an effective solution for the OUU problem. For this purpose, we have opted for the recently introduced graph-accelerated NIPC approach. This method combines the integration-based NIPC method with the computational graph transformation method known as AMTC, presenting a promising approach

Table 1 MDO problem formulation

	Description	Range (units)	Quantity
Objective	Aircraft total weight	w (kg)	1
Design variables	Wing span scaling	$-10 \leq b_w \leq 10$	1
	Tail span scaling	$-4 \leq b_t \leq 4$	1
	Tail incidence	$-10 \leq i_{ht} \leq 10$ (deg)	1
	Pitch angle	$-10 \leq \theta \leq 10$ (deg)	1
	Mach number	$0.1 \leq m \leq 0.3$	1
	Rotor speed	$500 \leq n \leq 3000$(rpm)	1
	Aperture diameter	$0.25 \leq d_a \leq 1$ (m)	1
	Wing beam cap thickness	$0.001 \leq t_{\text{cap}} \leq 0.01$(m)	14
	Wing beam web thickness	$0.001 \leq t_{\text{web}} \leq 0.01$ (m)	14
			Total design variables: 35
Constraints	Optical power residual	$r_{\text{o}} \geq 0$	1
	Trim residual	$r(\dot{\vec{x}}) \leq 1e^{-6}$	1
	Maximum stress	$s \leq s_{\max}$	70
			Total constraints: 72

to enhance computational efficiency in addressing the OUU problems with multi-disciplinary models.

1. Integration-based non-intrusive polynomial chaos

Polynomial chaos expansion (PCE), was originally introduced by Wiener, who used Hermite polynomials to develop a physical theory for Gaussian random processes [24]. Building on this, Ghanem applied Hermite polynomials as an orthogonal basis for random process representation [25]. Despite its advancements, PCE faces convergence challenges when dealing with non-Gaussian uncertain inputs. To address this, Xiu and Karniadakis introduced the generalized polynomial chaos (gPC) method [26], utilizing various orthogonal polynomials tailored to the distinct distributions of uncertain inputs to achieve optimal convergence for various UQ tasks.

Consider an uncertainty quantification (UQ) problem involving a function defined as follows:

$$f = \mathcal{F}(u), \tag{2}$$

where $\mathcal{F} : \mathbb{R}^d \to \mathbb{R}$ is the model's evaluation function, with $u \in \mathbb{R}^d$ as the input vector and $f \in \mathbb{R}$ as the scalar output. The uncertainties in the inputs are denoted as a stochastic vector, $U := [U_1, \ldots, U_d]$, assuming that these variables are independent. The stochastic input vector U conforms to a probability distribution $\rho(u)$, with support, Γ. The objective of this UQ problem is to calculate the statistical moments of the output random variable $f(U)$.

In gPC, the stochastic output, $f(U)$, can be approximated as a truncated series of orthogonal polynomials of the uncertain input variables:

$$f(U) = \sum_{i=0}^{n} \alpha_i \Phi_i(U), \tag{3}$$

where $\Phi_i(U)$ are the PCE basis functions and α_i are the corresponding PCE coefficients that need to be determined. The PCE basis functions are chosen based on the probability distribution of the uncertain inputs and they satisfy the orthogonality property as

$$\left\langle \Phi_i(U), \Phi_j(U) \right\rangle = \delta_{ij}, \tag{4}$$

where δ_{ij} is Kronecker delta and the inner product is defined as

$$\left\langle \Phi_i(U), \Phi_j(U) \right\rangle = \int_\Gamma \Phi_i(u)\Phi_j(u)\rho(u)du. \tag{5}$$

There are mainly two approaches to solving the PCE coefficients α_i: by integration or regression. On low-dimensional UQ problems, these two approaches have shown similar performance [27]. We consider the integration approach, which

Table 2 OUU problem formulation

	Description	Range (units)	Quantity
Objective	Aircraft total weight	$\mu_W + 3\sigma_W$ (kg)	1
Design variables	Wing span scaling	$-10 \leq b_w \leq 10$	1
	Tail span scaling	$-4 \leq b_t \leq 4$	1
	Tail incidence	$-10 \leq i_{ht} \leq 10$ (deg)	1
	Pitch angle	$-10 \leq \theta \leq 10$ (deg)	1
	Mach number	$0.1 \leq m \leq 0.3$	1
	Rotor speed	$500 \leq n \leq 3000$(rpm)	1
	Aperture diameter	$0.25 \leq d_a \leq 1$ (m)	1
	Wing beam cap thickness	$0.001 \leq t_{\text{cap}} \leq 0.01$(m)	14
	Wing beam web thickness	$0.001 \leq t_{\text{web}} \leq 0.01$ (m)	14
			Total design variables: 35
Random variables	Altitude	$\mathcal{U}(4000, 6000)$ (m)	1
	Horizontal distance	$\mathcal{U}(220, 280)$ (km)	1
	Payload weight	$\mathcal{U}(40, 60)$ (kg)	1
			Total random variables: 3
Constraints	Optical power residual	$\mu_{R_o} - 3\sigma_{R_o} \geq 0$	1
	Trim residual	$\mu_R + 3\sigma_R \leq 1e^{-6}$	1
	Maximum stress	$\mu_S + 3\sigma_S \leq S_{\max}$	70
			Total constraints: 72

makes use of the orthogonality property of PCE basis functions in (4). This approach projects the random output onto each basis function, which results in an integration problem to solve each coefficient:

$$\begin{aligned}\alpha_i &= \frac{\left\langle f(U), \Phi_i \right\rangle}{\left\langle \Phi_i^2 \right\rangle} \\ &= \int_\Gamma f(u)\Phi_i(u)\rho(u)du \\ &= \int_{\Gamma_1} \dots \int_{\Gamma_d} f(u_1, \dots, u_d)\Phi_i(u_1, \dots, u_d)\rho(u_1, \dots, u_d)du_1 \dots du_d.\end{aligned} \tag{6}$$

For low-dimensional UQ problems, the multi-dimensional integral in (6) is often approximated using the full-grid quadrature rule, as

$$\begin{aligned}\alpha_i &= \frac{1}{\left\langle \Phi_i^2 \right\rangle} \int_{u_1} \dots \int_{u_d} f(u_1, \dots, u_d)\Phi_k(u_1, \dots, u_d)\rho(u_1, \dots, u_d)du_1 \dots du_d \\ &\approx \frac{1}{\left\langle \Phi_i^2 \right\rangle} \sum_{i_1=0}^{k} \dots \sum_{i_d=0}^{k} w_1^{(i_1)} \dots w_d^{(i_d)} f(u_1^{(i_1)}, \dots, u_d^{(i_d)})\Phi_i(u_1^{(i_1)}, \dots, u_d^{(i_d)}),\end{aligned} \tag{7}$$

where $(u_i^{(1)}, \dots, u_i^{(k)})$ and $(w_i^{(1)}, \dots, w_i^{(k)})$ are the nodes and weights for the 1D Gauss quadrature rule with k nodes in the u_i dimension.

Once the PCE coefficients are determined, the mean and standard deviation of the random output can be analytically computed as follows:

$$\mu_f = \alpha_0, \tag{8}$$

$$\sigma_f = \sum_{i=1}^{d} \alpha_i^2. \tag{9}$$

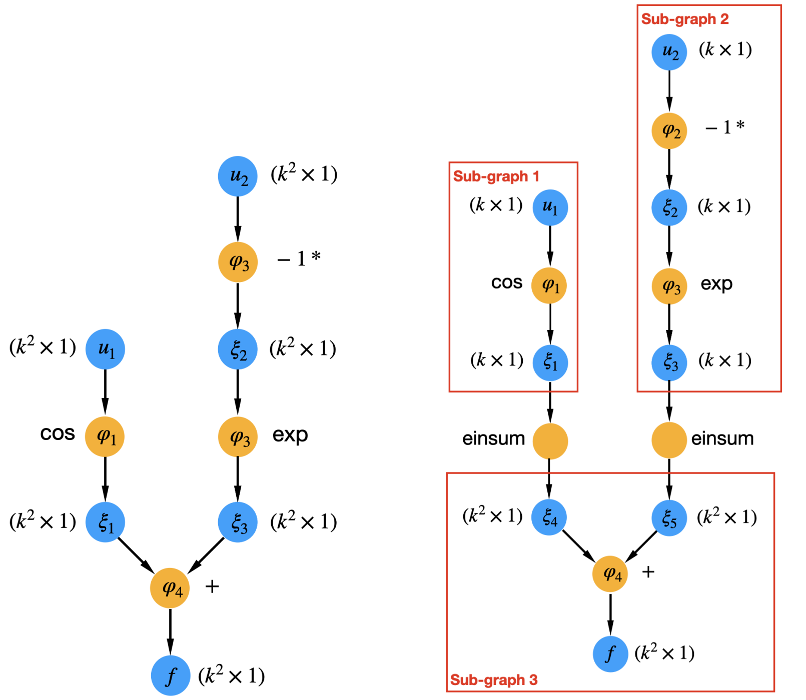

(a) Computational graph without using AMTC

(b) Computational graph using AMTC

Fig. 7 Computational graphs with data size for full-grid input points evaluation on $f = cos(u_1) + exp(-u_2)$

2. Accelerated model evaluations on tensor-grid using computational graph transformation

When using the full-grid quadrature rule to estimate the PCE coefficients as in (7), we need to evaluate the model output at the tensor-product quadrature points, which are defined as

$$\boldsymbol{u} = \boldsymbol{u}_1^k \times \cdots \times \boldsymbol{u}_d^k, \tag{10}$$

where

$$\boldsymbol{u}_i^k := \{u_i^{(j)}\}_{j=1}^k. \tag{11}$$

In this approach, the total number of quadrature points increases exponentially with the dimension of the UQ problem, as k^d. As a result, this is often favored only in low-dimensional problems. However, a recently proposed method, the Accelerated Model evaluations on Tensor grids using Computational graph transformations (AMTC) method [20, 21], finds a particular advantage in preserving the tensor structure of the input points. The AMTC method accelerates the model evaluations on tensor-grid inputs via a computational graph transformation approach. The main idea of AMTC is that when we view a computational model as a computational graph with elementary operations, each operation's output only has distinct evaluations on the distinct nodes in the space of its dependent input. When evaluating a model on tensor-grid input nodes, many operations may only depend on a small number of the uncertain inputs and the traditional framework to run the entire model in a for-loop approach creates many repeated evaluations on the operation level. The AMTC method eliminates repeated evaluations on the operation level by generating a modified computational graph based on the dependency information of the operations. In the modified computational graph, each operation is only evaluated on the distinct nodes in space of its dependent inputs. We show the comparison of the computational graphs with and without using AMTC in Fig. 7 when estimating a simple function $f = cos(u_1) + exp(-u_2)$ on tensor-grid inputs $\boldsymbol{u} = \boldsymbol{u}_1^k \times \boldsymbol{u}_2^k$.

The AMTC method has been implemented in the middle end of the compiler for a recently developed modeling language, Computational System Design Language (CSDL) [10] and has been well-connected to the integration-based NIPC to efficiently solve UQ problems involving multi-disciplinary and multi-point models. Several extensions of this method have been proposed to tackle UQ problems in different scenarios [28–30].

Table 3 Sparsity ratio of the uncertain inputs

Uncertain inputs	Sparsity ratio
Altitude	98.3%
Horizontal distance	0.4%
Payload weight	3.2%

B. Graph-accelerated NIPC for OUU

The application of the graph-accelerated NIPC method to solve an UQ problem involves a three-step process:

1) Generation of tensor-grid inputs based on the distribution of uncertain inputs.
2) Creation of a modified computational graph using AMTC.
3) Evaluation of the modified computational graph on tensor-grid inputs and subsequent post-processing of the model evaluations.

In the OUU context, the UQ problems at different optimization iterations involve the same computational graph and uncertain inputs but with different design variable values. Consequently, there's no need to regenerate the modified computational graph for each optimization iteration. Instead, we only need to update the design variable values on the modified computational graph at each optimization iteration. As a result, using the graph-accelerated NIPC approach to solve the OUU problem barely adds up any computational cost, and the acceleration it brought is directly related to the reduced repeated evaluations on the operation level.

IV. Numerical results

In this study, we first investigate the performance of the graph-accelerated NIPC method by applying it to the solution of the UQ problem with the initial design of the aircraft. We then compare its performance with integration-based NIPC and regression-based NIPC methods. The UQ results are also used to decide on the number of quadrature points we use in the OUU problem. Following this, we tackle an MDO problem, as outlined in Tab.1, aimed at refining the aircraft's initial design. After optimizing the design through MDO, this improved design serves as the starting point for addressing the OUU problem, detailed in Tab.2. We then draw a comparison between the results of the MDO and OUU, evaluating them across various metrics. This comparison underscores the effectiveness of the AMTC method. To ensure an equitable comparison in terms of computational time, we opt for the finite-difference approach to calculate gradients for all involved optimization problems.

A. Comparison of the UQ methods

We assess the performance of the graph-accelerated NIPC method by conducting a comparative analysis against two other UQ techniques. The objective here is to compute the mean and standard deviation of the objective function for the initial design of the aircraft, under the effect of the three uncertain inputs we defined. The three methods under evaluation are full-grid integration-based NIPC (integration-based NIPC), full-grid integration-based NIPC with AMTC (integration-based NIPC with AMTC) and regression-based NIPC. The regression-based NIPC results are generated using the software package Chaospy [31], with a random sampling approach.

The convergence plots of the UQ methods are shown in Fig. 8. The results here show that by using the AMTC method, the model evaluation cost of the integration-based NIPC method can be reduced by more than one order of magnitude making it the clear winner compared to the other two implemented methods. The significant acceleration here can be explained by looking at the sparsity ratio of each uncertain input shown in Tab. 3. The sparsity ratio was first introduced in [29] as a measure for the percentage of dependent computational cost for each uncertain input. From it, we observe that, out of the three uncertain inputs, two of them have only a small percentage of the computational cost dependent on them. This means, that most of the computationally dominant operations in this model are only dependent on one uncertain input, and only need to be evaluated on the k quadrature points in that dimension. By eliminating the redundant evaluations on the operation level, AMTC significantly accelerates the model evaluations on the tensor-grid.

B. Comparison of the MDO and OUU results

Based on the UQ results, we choose to use the integration-based NIPC to solve the UQ sub-problem in OUU. The full-grid Gauss quadrature points with 3 nodes in each dimension are used to ensure a balance between accuracy and

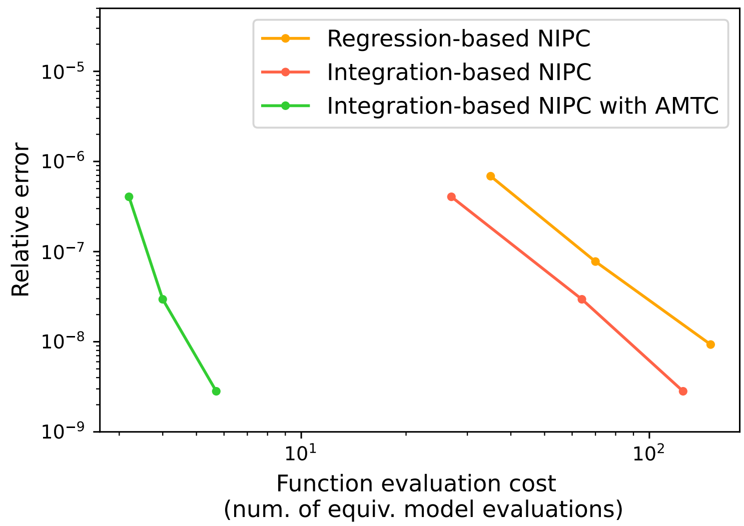

(a) Mean of the output

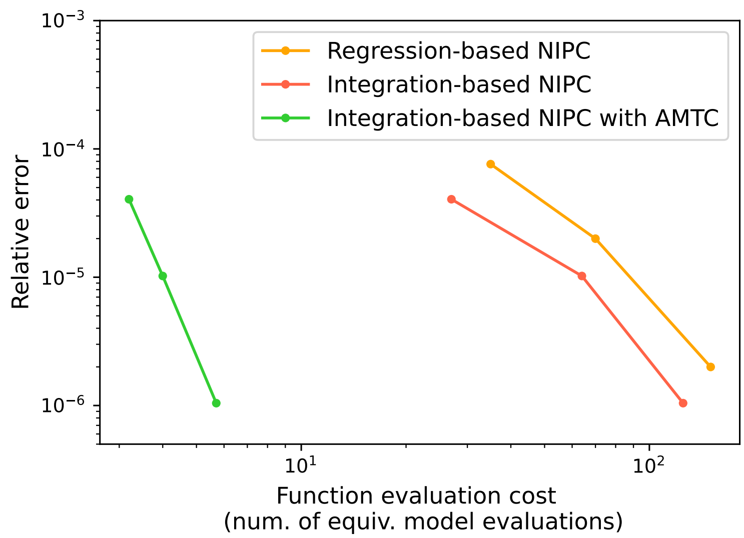

(b) Standard deviation of the output

Fig. 8 Convergence plots of the UQ methods

efficiency, and the AMTC method is used to accelerate the model evaluations on tensor-grid quadrature points.

The MDO and OUU-optimized designs are compared with the initial design in Tab. 4, and the visualization of MDO and OUU-optimized designs can be found in Fig. 9. The results reveal a notable distinction between the MDO-optimized design and the initial design. It is noteworthy that the MDO problem required 38 minutes for the optimizer to converge, leading to a significant enhancement over the initial design. Specifically, it resulted in a 40% reduction in the MDO objective function while satisfying all MDO constraints.

However, upon evaluating the OUU constraint functions on the MDO-optimized design, we discovered that four constraints were violated, with an average violation of approximately 1.2%. This implies that the MDO-optimized design may not fully comply with certain constraint functions when subjected to changes in flight conditions. Consequently, by employing OUU to enhance the MDO-optimized design, we achieved an optimal design that successfully meets all of the OUU constraint functions. While the OUU-optimized design exhibits a higher objective value compared to the MDO-optimized design, the fact that it satisfies all OUU constraints underscores its resilience when operating under varying flight conditions, characterized as uncertain inputs in the OUU problem. The comparison between MDO and OUU results under the effect of the uncertain inputs in one of the stress constraint functions that the MDO-optimized design violated is shown in Fig. 10. The results show that almost half of the probability density distribution for the MDO-optimized design is over the maximum stress limit while the entire distribution of the OUU-optimized design is below the maximum stress limit. Furthermore, in terms of computational efficiency in solving the OUU problem, the AMTC method plays a crucial role by reducing the total optimization time by approximately fivefold. Consequently, the optimization time for solving the OUU problem is merely twice that of solving the MDO problem

From an aircraft design perspective, it's worth noting that the OUU-optimized design exhibits distinct characteristics compared to the MDO-optimized counterpart. Specifically, the OUU-optimized design features a larger wing span, a greater tail span, and a generally thicker beam cross-section. These design differences can be attributed to the inherent conservatism of the OUU approach. The larger wing area in the OUU-optimized design is strategically designed to generate sufficient lift, ensuring the aircraft can carry potentially heavier payloads. Additionally, the stronger wing structure is designed to guarantee compliance with constraint requirements under a wide range of flight conditions. In summary, the OUU-optimized design prioritizes robustness and reliability across varying scenarios, which leads to these specific design modifications.

Table 4 Comparison of MDO and OUU results

	Initial design	MDO-optimized design	OUU-optimized design
Design variables:			
b_w	0	0.1145	0.1886
b_t	0	0.3149	0.3313
i_{ht}	0	1.674	1.573
θ	0	-0.3495	-0.5340
m	0.15	0.1	0.1
n	1500	1083	1082
d_a	0.75	0.5318	0.5368
MDO objective	1024	588	607
MDO constraints:			
Violation No.	19	0	0
Average violation (%)	>100%	-	-
OUU objective	1123	634	655
OUU constraints:			
Violation No.	20	4	0
Average violation (%)	>100%	1.2%	-
Number of opt. iterations	-	58	26
Optimization time	-	38 min	1h 18 min (with AMTC) 7h 52 min (without AMTC)

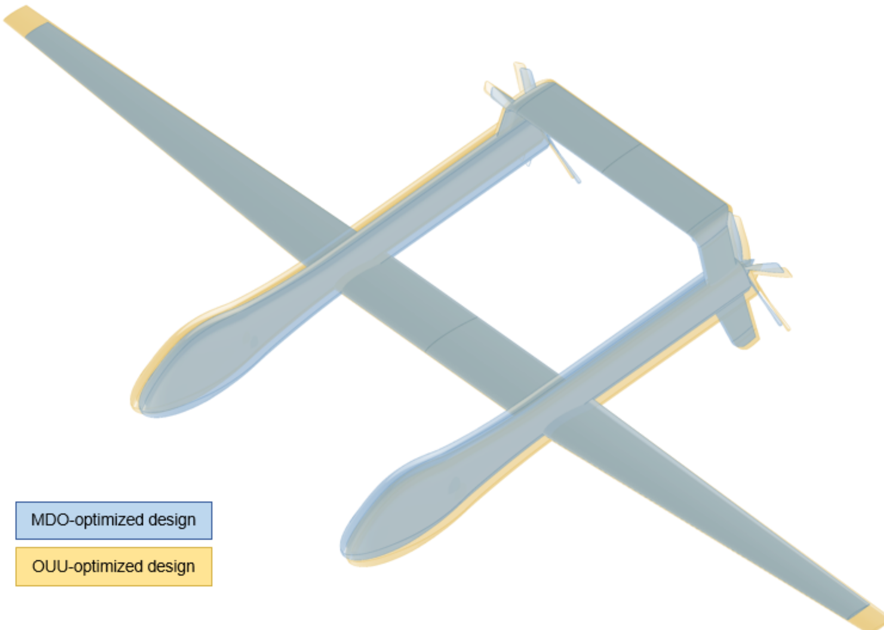

Fig. 9 Visualizations of the MDO and OUU results

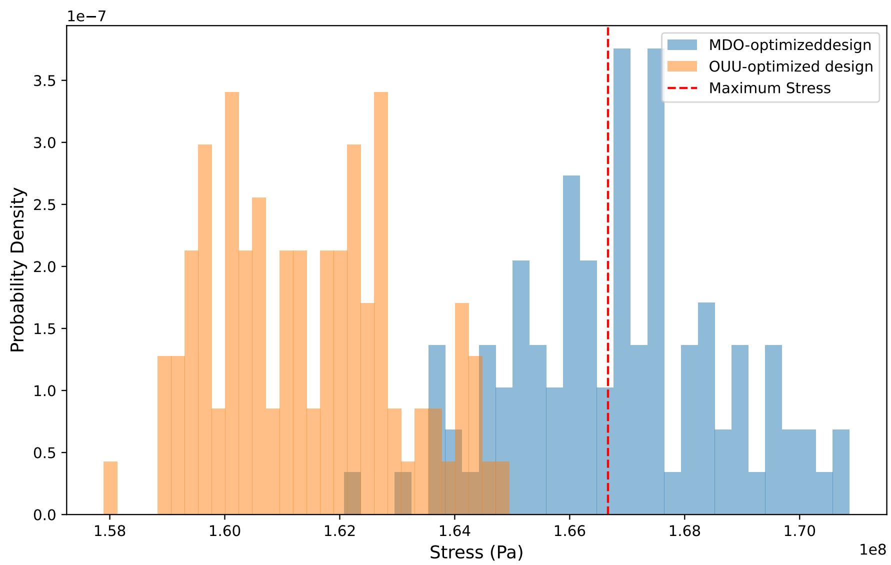

Fig. 10 Comparison of the probability density distributions of a stress constraint function output

V. Conclusion

In this paper, we applied a graph-accelerated non-intrusive polynomial chaos (NIPC) method to solve an optimization under uncertainty (OUU) problem derived from a laser-beam-powered aircraft design scenario. Numerical results show that the computational graph transformation method, AMTC, reduced the total optimization time by a factor of five, making the OUU problem computationally as twice as expensive as solving the MDO problem. The optimal design obtained from solving the OUU problem improved upon the optimal design obtained from solving the MDO problem by satisfying robust constraint functions, whereas the MDO-optimized design violated four of the robust constraints. In general, the OUU-optimized design exhibits a more conservative design approach compared to the MDO-optimized counterpart. This conservatism enhances its robustness and reliability, particularly in accommodating variations in the operating conditions.

In summary, our research underscores the advantages of solving the OUU problem to improve upon the MDO-optimized design, and also the notable efficiency gains achieved through the application of graph-accelerated NIPC for addressing large-scale multidisciplinary design optimization under uncertainty problems.

Acknowledgments

The material presented in this paper is, in part, based upon work supported by DARPA under grant No. D23AP00028-00

References

[1] Kenway, G., and Martins, J. R., "Aerostructural shape optimization of wind turbine blades considering site-specific winds," *12th AIAA/ISSMO multidisciplinary analysis and optimization conference*, 2008, p. 6025. https://doi.org/10.2514/6.2008-6025.

[2] Sarojini, D., Ruh, M. L., Joshy, A. J., Yan, J., Ivanov, A. K., Scotzniovsky, L., Fletcher, A. H., Orndorff, N. C., Sperry, M., Gandarillas, V. E., et al., "Large-Scale Multidisciplinary Design Optimization of an eVTOL Aircraft using Comprehensive Analysis," *AIAA SCITECH 2023 Forum*, 2023, p. 0146. https://doi.org/10.2514/6.2023-0146.

[3] McAllister, C. D., and Simpson, T. W., "Multidisciplinary robust design optimization of an internal combustion engine," *J. Mech. Des.*, Vol. 125, No. 1, 2003, pp. 124–130. https://doi.org/10.1115/detc2001/dac-21124.

[4] Kodiyalam, S., Yang, R., Gu, L., and Tho, C.-H., "Multidisciplinary design optimization of a vehicle system in a scalable, high performance computing environment," *Structural and Multidisciplinary Optimization*, Vol. 26, No. 3-4, 2004, pp. 256–263. https://doi.org/10.1007/s00158-003-0343-2.

[5] Ning, A., and Dykes, K., "Understanding the benefits and limitations of increasing maximum rotor tip speed for utility-scale wind turbines," *Journal of physics: conference series*, Vol. 524, IOP Publishing, 2014, p. 012087. https://doi.org/10.1088/1742-6596/524/1/012087.

[6] Balesdent, M., Bérend, N., Dépincé, P., and Chriette, A., "A survey of multidisciplinary design optimization methods in launch vehicle design," *Structural and Multidisciplinary optimization*, Vol. 45, No. 5, 2012, pp. 619–642. https://doi.org/10.1007/s00158-011-0701-4.

[7] Jilla, C., and Miller, D., "A multiobjective, multidisciplinary design optimization methodology for the conceptual design of distributed satellite systems," *9th AIAA/ISSMO Symposium on Multidisciplinary Analysis and Optimization*, 2002, p. 5491. https://doi.org/10.2514/6.2002-5491.

[8] Hwang, J. T., Lee, D. Y., Cutler, J. W., and Martins, J. R., "Large-scale multidisciplinary optimization of a small satellite's design and operation," *Journal of Spacecraft and Rockets*, Vol. 51, No. 5, 2014, pp. 1648–1663. https://doi.org/10.2514/1.a32751.

[9] Gray, J. S., Hwang, J. T., Martins, J. R., Moore, K. T., and Naylor, B. A., "OpenMDAO: An open-source framework for multidisciplinary design, analysis, and optimization," *Structural and Multidisciplinary Optimization*, Vol. 59, No. 4, 2019, pp. 1075–1104. https://doi.org/10.2514/6.2010-9101.

[10] Gandarillas, V., Joshy, A. J., Sperry, M. Z., Ivanov, A. K., and Hwang, J. T., "A graph-based methodology for constructing computational models that automates adjoint-based sensitivity analysis," *Structural and Multidisciplinary Optimization*, under revision.

[11] Yao, W., Chen, X., Luo, W., Van Tooren, M., and Guo, J., "Review of uncertainty-based multidisciplinary design optimization methods for aerospace vehicles," *Progress in Aerospace Sciences*, Vol. 47, No. 6, 2011, pp. 450–479. https://doi.org/10.1016/j.paerosci.2011.05.001.

[12] Keshavarzzadeh, V., Fernandez, F., and Tortorelli, D. A., "Topology optimization under uncertainty via non-intrusive polynomial chaos expansion," *Computer Methods in Applied Mechanics and Engineering*, Vol. 318, 2017, pp. 120–147. https://doi.org/10.1016/j.cma.2017.01.019.

[13] Kim, N. H., Wang, H., and Queipo, N. V., "Efficient shape optimization under uncertainty using polynomial chaos expansions and local sensitivities," *AIAA journal*, Vol. 44, No. 5, 2006, pp. 1112–1116. https://doi.org/10.2514/1.13011.

[14] Bedonian, G., and Hicken, J. E., "An Adaptive Sampling Method for Gradient-Enhanced Surrogate Modeling," *AIAA AVIATION 2022 Forum*, 2022, p. 3998. https://doi.org/10.2514/6.2022-3998.

[15] Rumpfkeil, M. P., "Optimizations under uncertainty using gradients, Hessians, and surrogate models," *AIAA journal*, Vol. 51, No. 2, 2013, pp. 444–451. https://doi.org/10.2514/1.J051847.

[16] Lim, D., and Yee, K., "Sizing for Advanced Air Mobility under Uncertainty Environment," *AIAA AVIATION 2023 Forum*, 2023, p. 4265. https://doi.org/10.2514/6.2023-4265.

[17] Chaudhuri, A., Jasa, J., Martins, J. R., and Willcox, K. E., "Multifidelity optimization under uncertainty for a tailless aircraft," *2018 AIAA Non-Deterministic Approaches Conference*, 2018, p. 1658. https://doi.org/10.2514/6.2018-1658.

[18] Ng, L. W.-T., and Eldred, M., "Multifidelity uncertainty quantification using non-intrusive polynomial chaos and stochastic collocation," *53rd aiaa/asme/asce/ahs/asc structures, structural dynamics and materials conference 20th aiaa/asme/ahs adaptive structures conference 14th aiaa*, 2012, p. 1852. https://doi.org/10.2514/6.2012-1852.

[19] Panda, K., and Hicken, J. E., "Hessian-based dimension reduction for optimization under uncertainty," *2018 Multidisciplinary Analysis and Optimization Conference*, 2018, p. 3102. https://doi.org/10.2514/6.2018-3102.

[20] Wang, B., Sperry, M., Gandarillas, V. E., and Hwang, J. T., "Accelerating model evaluations in uncertainty propagation on tensor grids using computational graph transformations," *arXiv preprint arXiv:2309.06617*, 2023. https://doi.org/10.48550/arXiv.2309.06617.

[21] Wang, B., Sperry, M., Gandarillas, V. E., and Hwang, J. T., "Efficient uncertainty propagation through computational graph modification and automatic code generation," *AIAA AVIATION 2022 Forum*, 2022, p. 3997. https://doi.org/10.2514/6.2022-3997.

[22] Orndorff, N. C., Wang, B., Ruh, M. L., Fletcher, A., and Hwang, J. T., "Gradient-based sizing optimization of power-beaming-enabled aircraft," *AIAA AVIATION 2023 Forum*, 2023, p. 4019. https://doi.org/10.2514/6.2023-4019.

[23] Fiorino, S. T., Randall, R. M., Bartell, R. J., Haiducek, J. D., Spencer, M. F., and Cusumano, S. J., "Field measurements and comparisons to simulations of high energy laser propagation and off-axis scatter," *Free-Space Laser Communications X*, Vol. 7814, SPIE, 2010, pp. 186–196. https://doi.org/10.1117/12.860046.

[24] Wiener, N., "The homogeneous chaos," *American Journal of Mathematics*, Vol. 60, No. 4, 1938, pp. 897–936. https://doi.org/10.2307/2371268.

[25] Ghanem, R., "Ingredients for a general purpose stochastic finite elements implementation," *Computer methods in applied mechanics and engineering*, Vol. 168, No. 1-4, 1999, pp. 19–34. https://doi.org/10.1016/S0045-7825(98)00106-6.

[26] Xiu, D., and Karniadakis, G. E., "The Wiener–Askey polynomial chaos for stochastic differential equations," *SIAM journal on scientific computing*, Vol. 24, No. 2, 2002, pp. 619–644. https://doi.org/10.1137/S1064827501387826.

[27] Eldred, M., and Burkardt, J., "Comparison of non-intrusive polynomial chaos and stochastic collocation methods for uncertainty quantification," *47th AIAA aerospace sciences meeting including the new horizons forum and aerospace exposition*, 2009, p. 976. https://doi.org/10.2514/6.2009-976.

[28] Wang, B., Orndorff, N. C., and Hwang, J. T., "Optimally tensor-structured quadrature rule for uncertainty quantification," *AIAA SCITECH 2023 Forum*, 2023, p. 0741. https://doi.org/10.2514/6.2023-0741.

[29] Wang, B., Orndorff, N. C., Sperry, M., and Hwang, J. T., "High-dimensional uncertainty quantification using graph-accelerated non-intrusive polynomial chaos and active subspace methods," *AIAA AVIATION 2023 Forum*, 2023, p. 4264. https://doi.org/10.2514/6.2023-4264.

[30] Wang, B., Orndorff, N. C., Sperry, M., and Hwang, J. T., "A gradient-enhanced univariate dimension reduction method for uncertainty propagation," *AIAA SCITECH 2024 Forum*, 2024.

[31] Feinberg, J., and Langtangen, H. P., "Chaospy: An open source tool for designing methods of uncertainty quantification," *Journal of Computational Science*, Vol. 11, 2015, pp. 46–57. https://doi.org/10.1016/j.jocs.2015.08.008.